

Submitted to *The Astrophysical Journal* on June 5, 2001  
 Revised: July 24, 2001

## Radiation from collision-dominated relativistic pair fireballs

M. Böttcher<sup>1</sup>

*Department of Physics and Astronomy, Rice University, MS 108,  
 6100 S. Man Street, Houston, TX 77005 - 1892, USA*

mboett@spacsun.rice.edu

R. Schlickeiser

*Institut für Theoretische Physik, Lehrstuhl IV  
 Ruhr-Universität Bochum, D-44780 Bochum, Germany*

rsch@egal.tp4.ruhr-uni-bochum.de

and

A. Marra<sup>2</sup>

*Stephen F. Austin High School, 3434 Pheasant Creek Drive,  
 Sugar Land, TX 77478, USA*

anibal.marra@cognitas.com

### ABSTRACT

It is generally accepted that gamma-ray bursts (GRBs) are initiated by a relativistic pair fireball, converting its internal energy into kinetic energy of a relativistically moving plasmoid and subsequently into radiation. Here, we investigate the early stages of this evolution, after the pair fireball has become optically thin to  $\gamma\gamma$  pair production. We show that for a short period of time,  $\sim 0.1$  – a few seconds after the initial explosion, the pair plasmoid evolution might be dominated by collisional processes prior to the formation of a collisionless shock. We simulate these processes during the early pair plasmoid evolution and calculate the expected radiative signatures. We show that the radiation from the collision-dominated pair plasmoid phase results in a short ( $\sim$  a few ms) flash of thermal soft X-ray emission, followed by a transition phase of  $\lesssim 1$  s during which

the fireball turns Thomson thin, but its radiation remains dominated by thermal Comptonization, peaking at around  $E_{\text{pk}} \sim 100$  MeV – a few GeV. While the very early thermal emission could be associated with the quasi-thermal radiation signatures found in the very early phases of several bright BATSE GRBs, the predicted subsequent flash of high-energy emission should be easily detectable with the GLAST satellite.

*Subject headings:* gamma rays: bursts — gamma-rays: theory

## 1. Introduction

With the establishment of the cosmological distance scale of  $\gamma$ -ray bursts (GRBs) and the considerable success of the synchrotron-shock model (Mészáros & Rees 1993; Katz 1994; Tavani 1996) to explain the broadband (radio through X-ray) continuum afterglow signatures of GRBs (Wijers, Rees, & Mészáros 1997; Vietri 1997; Waxman 1997; Galama et al. 1998; Mészáros, Rees, & Wijers 1998), it is now generally accepted that GRBs are initiated by a relativistic pair fireball, transferring its internal energy into kinetic energy of a relativistic blast wave (Cavallo & Rees 1978; Shemi & Piran 1990; Mészáros & Rees 1992; Rees & Mészáros 1992). Non-thermal particle acceleration at the forward shock and subsequent radiative cooling is believed to lead to the formation of a broken power-law distribution of ultrarelativistic electrons, producing the observed broadband afterglow radiation primarily through synchrotron emission (e.g., Sari, Piran, & Narayan (1998); Böttcher & Dermer (2000)), though Compton upscattering of synchrotron photons may also play a significant role (Dermer, Böttcher, & Chiang 2000; Sari & Esin 2001).

In the relativistic fireball/blastwave model for GRBs, a large amount of energy is released in a short period of time. This initial configuration is highly opaque to  $\gamma\gamma$  absorption and pair production and leads to the formation of a relativistic pair fireball. As the fireball expands, it cools adiabatically, converting its internal energy into bulk kinetic energy of the outflow, and its  $\gamma\gamma$  opacity decreases until it becomes optically thin to  $\gamma\gamma$  pair production. At this time, the pairs are essentially cold in a reference frame co-moving with a small section of the expanding pair plasma / radiation shell. It has been recognized very early-on (e.g., Shemi & Piran (1990); Mészáros & Rees (1992)) that even a small intrinsic or external

---

<sup>1</sup>Chandra Fellow

<sup>2</sup>Current address: MIT, School of Engineering; 77 Massachusetts Avenue; Cambridge, MA 02139-4307

contamination of the pair fireball with baryons would lead to re-conversion of most of the fireball energy into kinetic energy of the outflow, and that any radiation escaping the pair fireball during this phase of energy conversion would have quasi-thermal signatures.

However, more detailed measurements of time-averaged photon spectra emerging from GRBs, in particular by the Burst and Transient Source Experiment (BATSE) on board the *Compton Gamma-Ray Observatory* (CGRO) have shown that they can generally be fitted successfully with a model consisting of two power-laws, smoothly connected by an exponential turn-over (Band et al. 1993). Such a power-law high-energy spectrum was interpreted as the radiative signature of non-thermal particle acceleration at relativistic shocks formed in the process of deceleration of the relativistic blast wave produced during the initial fireball stage (e.g., Paczyński & Rhoads (1993); Mészáros & Rees (1993)). While it is now generally agreed that the smoothly decaying afterglow emission observed from many GRBs is produced by relativistic electrons accelerated at the external forward shock, in the stage when the blast wave is efficiently being decelerated by the sweeping-up of external material, many researchers now believe that the emission during the prompt GRB phase may be produced in internal shocks during collisions of subsequent relativistic blast waves produced in a series of energy release events from the central engine (e.g., Fenimore, Madras, & Nayakshin (1996); Sari & Piran (1997)), although an external-shock scenario for the prompt GRB phase cannot be ruled out at this time (e.g., Dermer & Mitman (1999)).

Both internal and external shock scenarios for GRBs are generally starting out with the assumption that the relativistic blast wave has produced a relativistic shock with fully developed hydromagnetic turbulence in order to allow for efficient non-thermal particle acceleration at the shock front. This neglects the fact that it takes a finite amount of time to build up the necessary turbulence in the two-stream multi-fluid system consisting of the relativistically moving pair plasma and the background hydrogen plasma. While a detailed treatment of the process of the development of hydromagnetic turbulence through a relativistic two-stream instability is rather cumbersome (see, e.g., Pohl & Schlickeiser (2000); Schlickeiser & Dermer (2000); Schlickeiser et al. (2001)), the time scale for the development of such turbulence can be estimated by the Alfvén crossing time through the shell of relativistically moving pair plasma. Using hydrodynamics simulations, Mészáros, Laruna, & Rees (1993) have demonstrated that a relativistic pair fireball becomes rapidly compressed into a shell of co-moving thickness  $\Delta'$  with  $R/\Delta' \sim \Gamma_0$  during the early evolution of the fireball, and that the ratio  $R/\Delta'$  remains approximately constant after this compression phase, as long as the blast wave is coasting (i.e.  $\Gamma \approx \text{const.}$ ). A relativistic pair fireball of this thickness, carrying a total energy per unit solid angle of  $E_\Omega = 10^{52} E_{\Omega,52} \text{ erg sr}^{-1} = m_e c^2 n'_{\text{pair}} R^3 = 8.2 \times 10^{52} n'_{14} R_{15}^3 \text{ erg sr}^{-1}$  is initially highly optically thick to Thomson scattering and thus radiatively inefficient since radiation will remain trapped within the

shell. Here,  $n'_{\text{pair}} = 10^{14} n'_{14} \text{ cm}^{-3}$  is the co-moving pair density (throughout the paper, primed quantities refer to the reference frame co-moving with the pair plasmoid), and  $R_{15} = 10^{15} R_{15} \text{ cm}$ , where  $\sim 10^{15} \text{ cm}$  is a typical value for the Thomson thinning radius (see §6). We assume that the magnetic field given by the equipartition parameter  $\epsilon_B = 0.1 \epsilon_{B,-1}$  between magnetic field and pair plasma energy density (i.e.,  $u'_B = \epsilon_B u'_{\text{pair}}$ ), and that the pair plasma is cold in the co-moving frame. Then, for a bulk Lorentz factor  $\Gamma = 10^3 \Gamma_3$ , the Alfvén crossing time scale in the observer’s frame is

$$t_A \sim 0.1 \frac{R_{15}}{\Gamma_3^2 \epsilon_{B,-1}^{1/2}} \text{ s}. \quad (1)$$

Thus, Eq. (1) indicates that it may take  $\sim 0.1 - 1 \text{ s}$ , i. e. a non-negligible fraction of the prompt GRB phase, to build up the hydromagnetic turbulence for non-thermal particle acceleration at either internal or external shocks associated with these pair blastwaves.

The time scale (in the observer’s frame) for collisional processes,  $t_{\text{coll}}$ , may be estimated as

$$t_{\text{coll}} \sim (\Gamma c n'_{\text{pair}} \sigma_T)^{-1} \sim 5 \times 10^{-4} (n'_{14} \Gamma_3)^{-1} \text{ s}, \quad (2)$$

indicating that during the initial phase — prior to the generation of strong hydromagnetic turbulence — the radiative and energy-exchange processes in the blast wave are dominated by collisional processes. This fact is particularly interesting in view of the evidence in a significant fraction of GRB that the early time-resolved BATSE spectra show too hard a low-energy spectrum to be produced by non-thermal synchrotron emission (Crider et al. 1997; Preece et al. 1998). Recently, Preece (2001) has found evidence in several BATSE GRBs that their very early spectra are described better by thermal rather than nonthermal emission.

Setting both time scales (1) and (2) equal, one can estimate the condition under which non-thermal particle acceleration may begin to dominate the particle energization behind the forward shock. We find that collisional processes will dominate as long as

$$\frac{t_A}{t_{\text{coll}}} \sim 24 \frac{E_{\Omega,52}}{\Gamma_3 R_{15}^2 \epsilon_{B,-1}^{1/2}} > 1. \quad (3)$$

Although alternative emission models for the prompt GRB radiation have been proposed by several authors (e.g., Brainerd (1994); Liang (1997)), the dynamics and radiative signatures of the transition phase between the time when the fireball becomes optically thin and the time of efficient non-thermal particle acceleration by hydromagnetic turbulence has not

been studied in detail. In this paper, we are simulating the evolution of and time-dependent emission from a relativistic pair plasmoid before the generation of hydromagnetic turbulence leading to non-thermal particle acceleration. In §2, we describe and motivate the basic assumptions of our model. The computation of the evolution of the thermal pair plasma and the fate of the swept-up background plasma are outlined in §3. In §4 we describe the calculation of the time-dependent radiation spectra emitted by the resulting particle distributions in the blast wave. The evaluation of the global dynamics of the blast wave is given in §5. Results of our numerical study are presented in §6. We summarize in §7.

## 2. Model setup

We assume that the pair plasmoid forming the blastwave is a circular shell segment with opening solid angle  $\Omega$ . Initially, it consists of a pure pair plasma with a pair density  $n'_{\text{pair}} = 10^{14} n'_{14} \text{ cm}^{-3}$  in the co-moving frame of the pair plasmoid. At the time when the pair fireball becomes optically thin to  $\gamma\gamma$  pair production, the pairs are essentially cold in the co-moving frame. The blastwave interacts with an external medium (normal electron-proton plasma) of density  $n_{\text{ISM}} = 1 n_{\text{ISM},0} \text{ cm}^{-3}$  in the stationary frame of the surrounding medium. At any given time, the plasmoid is located at a radius  $R = 10^{15} R_{15} \text{ cm}$  from the center of the explosion and has a thickness  $\Delta' = R/\Gamma$  in the co-moving frame. The bulk Lorentz factor of the plasmoid is denoted by  $\Gamma = 10^3 \Gamma_3$ . The background magnetic field in the blastwave is  $B = 1 B_0 \text{ G}$  and parametrized by the equipartition parameter  $\epsilon_B = \epsilon_{B,-1}$  through

$$B_0 = 1.4 \times 10^4 (\epsilon_{B,-1} n'_{14})^{1/2} \left( \frac{K_3 \left[ \frac{1}{\Theta_{\text{pair}}} \right]}{K_2 \left[ \frac{1}{\Theta_{\text{pair}}} \right]} - \Theta_{\text{pair}} \right)^{1/2} \quad (4)$$

where  $\Theta_{\text{pair}} = kT_{\text{pair}}/(m_e c^2)$  is the normalized (co-moving) pair temperature in the plasmoid, and  $K_n$  is the modified Bessel function of 2nd kind (a.k.a. McDonald function) of order  $n$ . For simplicity, we assume  $\epsilon_B$  to be constant throughout our simulation. In fact, a gradual build-up of the magnetic field from lower initial values of  $\epsilon_B$  may extend the period of applicability of our approach.

We are following the evolution of both the pair plasma as it is being energized by Coulomb and inelastic (i.e. bremsstrahlung) collisions with swept-up electrons and protons from the surrounding medium, and cools via radiative and adiabatic cooling. Simultaneously, we solve for the evolution of the population of suprathermal protons and electrons which are swept up from the environment with an initial Lorentz factor  $\Gamma$  in the co-moving frame of the plasmoid, and transfer their energy to the background pair plasma and into radiation.

### 3. Evolution of pairs, electrons and protons in the blastwave

Electrons and protons which are swept up by the pair blastwave have an initial Lorentz factor  $\Gamma$  in the co-moving frame, and will transfer part of their kinetic energy to the background pairs in the plasmoid via elastic scattering (Møller/Bhabha and Coulomb scattering, respectively), thus heating the thermal pair plasma. The remainder of the kinetic electron/proton energy will be radiated away through bremsstrahlung with the background plasma and through synchrotron radiation. The thermal background plasma will be heated by collisions with the swept-up electrons and protons and cool via bremsstrahlung and synchrotron emission, adiabatic losses and pair annihilation. The very short time scale for elastic scattering in the plasmoid (see Eq. [2]) indicates that the incoming particles are rapidly isotropized in the co-moving frame of the plasmoid. Thus, we assume local isotropy of the particle distributions.

#### 3.1. Suprathermal electron/proton cooling rates

In the following, we quote simple approximation formulae for the cooling rates for suprathermal electrons and protons in a cold background pair plasma, which will be used in our simulations to follow the evolution of the swept-up non-thermal particle distributions. For highly relativistic test particles, the elastic scattering cross sections for electron-electron (Møller) and electron-positron (Bhabha) scattering are approximately equal, and we may use a simple power-law fit to the Møller scattering energy exchange rate of a test particle with a cold background pair plasma given by Nayakshin & Melia (1998). We find

$$\dot{\gamma}_{\text{M}\ddot{o}\text{ller},e} \approx 2.6 \times 10^3 n'_{14} \gamma_e^{-0.02} \text{ s}^{-1}. \quad (5)$$

The  $e^-e^-$  and  $e^-e^+$  bremsstrahlung energy loss rate can be approximated as

$$\dot{\gamma}_{\text{br},e} \approx 8 \times 10^{-2} n'_{14} \gamma_e^{1.15} \text{ s}^{-1}. \quad (6)$$

Suprathermal electrons will also emit synchrotron radiation, thus losing energy at a rate

$$\dot{\gamma}_{\text{sy},e} \approx 1.29 \times 10^{-9} B_0^2 \gamma_e^2 \text{ s}^{-1}. \quad (7)$$

Finally, we take into account synchrotron-self-Compton emission and estimate the associated energy loss as

$$\dot{\gamma}_{\text{SSC},e} \approx -\frac{4}{3} c \sigma_T \frac{u'_{\text{sy},e}}{m_e c^2} \gamma_e^2 \quad (8)$$

where  $u'_{\text{sy}} \approx L'_{\text{sy},e}/(\Omega R^2 c)$  is the energy density in synchrotron photons. These estimates indicate that except for the highest-energy electrons (with  $\gamma_e \gtrsim 10^3$ ), the energy loss will be dominated by elastic scattering, leading to rapid thermalization of the suprathermal electrons.

For Coulomb losses of suprathermal protons in the cold pair plasma, we use Eq. (4.22) of Mannheim & Schlickeiser (1994) with  $\beta \gg \beta_e$  (i.e. ultrarelativistic protons in a non-relativistic or mildly relativistic background plasma):

$$\dot{\gamma}_{\text{Coul},p} \approx 3.3 \times 10^{-2} n'_{14} \text{ s}^{-1} \quad (9)$$

The bremsstrahlung energy loss rate of suprathermal protons is evaluated by integrating the respective photon spectrum calculated by citetjones71 over the outgoing photon energies. Since to our knowledge, the result has not yet been published elsewhere, we derive the complete expression in Appendix A. In our simulations, we use a simple power-law fit to the resulting bremsstrahlung energy loss rate:

$$\dot{\gamma}_{\text{br},p} \approx 1.1 \times 10^{-5} n'_{14} \gamma_p^{0.3} \text{ s}^{-1} \quad (10)$$

Finally, we take into account synchrotron emission of ultrarelativistic protons, leading to an energy loss of

$$\dot{\gamma}_{\text{sy},p} \approx \frac{c \sigma_T B^2}{6\pi m_p c^2} \left( \frac{m_e}{m_p} \right)^2 \gamma^2 \approx 2.09 \times 10^{-19} B_0^2 \gamma_p^2 \text{ s}^{-1}. \quad (11)$$

As in the case of suprathermal electrons, we expect that the swept-up protons will lose energy primarily via elastic scattering with the thermal background pair plasma.

### 3.2. Suprathermal electron and proton spectra

As mentioned in the previous section, we generally expect that the energy loss of both protons and electrons might be dominated by Coulomb interactions for  $\gamma_{p,\text{max}} = \Gamma \lesssim 10^3$ . However, for the highest-energy protons and electrons, synchrotron losses may also play an important role. The evolution of the suprathermal electron and proton populations may be calculated by solving the continuity equation for the cooling particles:

$$\frac{\partial N_e(\gamma, t')}{\partial t'} = -\frac{\partial}{\partial \gamma} (\dot{\gamma} N[\gamma, t']) + \dot{N}_{\text{sw}}(\gamma, t'), \quad (12)$$

where  $\dot{N}_{\text{sw}}(\gamma, t') = \beta_{\Gamma} c \Gamma n_{\text{ISM}} \Omega R^2 \delta(\gamma - \Gamma)$  is the sweep-up rate of ISM particles, and we have neglected escape. Since the cooling time scale for ultrarelativistic particles is of the order of or shorter than the dynamical time scale, we may approximate the evolution by a sequence of quasi-equilibrium solutions to Eq. (12), given by

$$N_e(\gamma_e) = N_e^0 \begin{cases} \left(\frac{\gamma_e}{\gamma_e^{\text{br}}}\right)^{0.02} & \text{for } 1 \leq \gamma_e \leq \gamma_e^{\text{br}} \\ \left(\frac{\gamma_e}{\gamma_e^{\text{br}}}\right)^{-2} & \text{for } \gamma_e^{\text{br}} \leq \gamma_e \leq \Gamma \end{cases} \quad (13)$$

for the electrons and

$$N_p(\gamma_p) = N_p^0 \begin{cases} 1 & \text{for } 1 \leq \gamma_p \leq \gamma_p^{\text{br}} \\ \left(\frac{\gamma_p}{\gamma_p^{\text{br}}}\right)^{-2} & \text{for } \gamma_p^{\text{br}} \leq \gamma_p \leq \Gamma \end{cases} \quad (14)$$

for the protons. The break energies are defined through the condition  $\dot{\gamma}_{\text{elast. scat.}} = \dot{\gamma}_{\text{sy}}$  and given by

$$\gamma_e^{\text{br}} = 8.5 \times 10^6 (n'_{14})^{\frac{1}{2.02}} B_0^{-\frac{1}{1.01}} \quad (15)$$

and

$$\gamma_p^{\text{br}} = 3.95 \times 10^8 (n'_{14})^{1/2} B_0^{-1}. \quad (16)$$

If  $\gamma_{e/p}^{\text{br}} \geq \Gamma$ , the high-energy branches of Eqs. (13) and (14) are not realized, and the respective particle spectra are single truncated power-laws for  $1 \leq \gamma_{e/p} \leq \Gamma$ .

The background pair plasma is assumed to maintain a thermal distribution at a temperature determined by the balance between heating by the swept-up particles and radiative cooling via bremsstrahlung and synchrotron emission.

### 3.3. Temperature of thermal pair plasma

As mentioned above, most of the kinetic energy of the protons is transferred to electrons through Coulomb collisions with the thermal background pair plasma. Thus, the heating rate of the thermal plasma is given by



$$L_{\text{heat}} = \Omega R^2 \Gamma^2 m_p c^2 \beta c n_{\text{ISM}} \approx 4.50 \times 10^{41} \Omega R_{15}^2 \Gamma_3^2 n_{\text{ISM},0} \text{ erg s}^{-1}. \quad (17)$$

This heating should be balanced by cooling through bremsstrahlung,

$$L_{\text{br,th}} \approx \begin{cases} 3.42 \times 10^{48} \Omega (n'_{14})^2 R_{15}^2 \Delta'_{12} \sqrt{\Theta_{\text{pair}}} \text{ erg s}^{-1} & \text{for } \Theta_{\text{pair}} \ll 1 \\ 1.36 \times 10^{49} \Omega (n'_{14})^2 R_{15}^2 \Delta'_{12} \Theta_{\text{pair}} (\ln[2\Theta_{\text{pair}}] + 0.673) \text{ erg s}^{-1} & \text{for } \Theta_{\text{pair}} \gtrsim 1 \end{cases} \quad (18)$$

— where  $\Delta'_{12} = \Delta'/(10^{12} \text{ cm})$  —, synchrotron emission,

$$L_{\text{sy,th}} \approx 3.175 \times 10^{41} \Omega n'_{14} R_{15}^2 \Delta'_{12} B_0^2 \Theta \frac{K_3(1/\Theta)}{K_2(1/\Theta)} \text{ erg s}^{-1} \quad (19)$$

(cf. Böttcher et al. (1999)), and thermal Comptonization of the soft photon field (at  $E \ll m_e c^2$ ). For typical parameters, the pair plasmoid is expected to be moderately optically thick,  $\tau_T \gtrsim 1$ , and have mildly relativistic temperatures,  $\Theta \lesssim 1$ . In this regime, we may use the analytic solution of Hua & Titarchuk (1995) for the saturated-Comptonization case (their Eq. [9]). We assume that the dominant soft input radiation field is the electron synchrotron component, which we approximate, for simplicity, by a  $\delta$  function spectrum  $L_s(\epsilon) = L_{\text{sy,e}} \delta(\epsilon - \epsilon_{\text{sy,e}}^{\text{max}})$ . The cooling rate due to Thermal Comptonization is then calculated by integrating the Comptonized spectrum (in the comoving frame) over photon energy.

Adiabatic cooling is described by a virtual luminosity  $L_{\text{adi}} = 3 E_{\text{th}} c/R$ , where  $E_{\text{th}}$  is the thermal energy content of the thermal pair plasma. At nonrelativistic pair plasma temperatures, pair annihilation becomes important. We use the expressions of Svensson (1982) for the pair annihilation cooling rate and the pair annihilation rate to calculate the cooling and depletion of the number of pairs due to this process.

#### 4. Radiation spectra

The radiation emitted by the thermal pair plasma can be calculated using standard expressions (see, e.g., Böttcher et al. (1999), and Hua & Titarchuk (1995) for the Thermal Comptonization component). The intrinsic luminosities of the bremsstrahlung and synchrotron components are given by Eqs. (18) and (19), respectively.

The (optically thin) bremsstrahlung spectrum of the suprathermal electrons in the comoving frame reproduces the broken power-law shape of the electron spectrum:

$$L'_{\text{br,e}}(\epsilon') = L_{\text{br,e}}^0 \begin{cases} 1 & \text{for } \epsilon' \leq \epsilon_{\text{br,e}}^{\text{br}} \\ \left(\frac{\epsilon'}{\epsilon_{\text{br,e}}^{\text{br}}}\right)^{-1} & \text{for } \epsilon_{\text{br,e}}^{\text{br}} \leq \epsilon' \leq \Gamma \end{cases} \quad (20)$$

where  $\epsilon_{\text{br,e}}^{\text{br}} = \gamma_e^{\text{br}}$  and  $\epsilon' = h\nu'/(m_e c^2)$ . The suprathermal proton bremsstrahlung spectrum may be approximated as

$$L'_{\text{br,p}}(\epsilon) = L_{\text{br,p}}^0 \begin{cases} 1 & \text{for } \epsilon' \leq \frac{1}{2} \\ (2\epsilon')^{-1.25} & \text{for } \frac{1}{2} \leq \epsilon' \leq \Gamma \end{cases} \quad (21)$$

(Jones 1971).

The nonthermal synchrotron spectra can be approximated as

$$L'_{\text{sy,e/p}}(\epsilon') = L_{\text{sy,e/p}}^0 \begin{cases} \left(\frac{\epsilon'}{\epsilon_{\text{sy,e/p}}^{\text{br}}}\right)^{1/3} & \text{for } \epsilon' \leq \epsilon_{\text{sy,e/p}}^{\text{br}} \\ \left(\frac{\epsilon'}{\epsilon_{\text{sy,e/p}}^{\text{br}}}\right)^{-1/2} & \text{for } \epsilon_{\text{sy,e/p}}^{\text{br}} \leq \epsilon' \leq \epsilon_{\text{sy,e/p}}^{\text{max}} \end{cases} \quad (22)$$

where

$$\epsilon_{\text{sy,e}}^{\text{br}} = \frac{B}{B_c} (\gamma_e^{\text{br}})^2 \quad (23)$$

$$\epsilon_{\text{sy,e}}^{\text{max}} = \frac{B}{B_c} \Gamma^2 \quad (24)$$

$$\epsilon_{\text{sy,p}}^{\text{br}} = \frac{3}{2} \frac{m_e}{m_p} \frac{B}{B_c} (\gamma_p^{\text{br}})^2 \quad (25)$$

$$\epsilon_{\text{sy,p}}^{\text{max}} = \frac{3}{2} \frac{m_e}{m_p} \frac{B}{B_c} \Gamma^2 \quad (26)$$

with  $B_c = 4.414 \times 10^{13}$  G.

Using a simple delta-function approximation for the Compton-scattering cross section in the Thomson limit, the evaluation of the electron-SSC spectrum is straightforward, but a bit lengthy. The full expression is given in Appendix B.

The normalization factors of the radiation spectra are given by setting the energy-integrated luminosities,

$$L_{\text{br},e} = L_{\text{br},e}^0 \epsilon_{\text{br},e}^{\text{br}} \left( 1 + \ln \left[ \frac{\Gamma}{\epsilon_{\text{br},e}^{\text{br}}} \right] \right) \quad (27)$$

$$L_{\text{br},p} = \frac{L_{\text{br},p}^0}{2} (1 + 4 [1 - (2\Gamma)^{-0.25}]) \quad (28)$$

$$L_{\text{sy},e/p} = L_{\text{sy},e/p}^0 \left( \frac{4}{3} \epsilon_{\text{sy},e/p}^{\text{br}} + 2 \sqrt{\epsilon_{\text{sy},e/p}^{\text{br}}} \left[ \sqrt{\epsilon_{\text{sy},e/p}^{\text{max}}} - \sqrt{\epsilon_{\text{sy},e/p}^{\text{br}}} \right] \right) \quad (29)$$

$$L_{\text{SSC},e} = L_{\text{SSC}}^0 N \quad (30)$$

where  $N$  is given in Appendix B (Eq. [B4]), equal to the fraction of swept-up kinetic particle energy, which is transferred into the respective radiative cooling channel,

$$L_{\text{br},e} = \Omega \Gamma^2 R^2 m_e c^2 \beta c n_{\text{ISM}} \frac{\dot{\gamma}_{\text{br},e}}{\dot{\gamma}_{\text{M}\emptyset,e} + \dot{\gamma}_{\text{br},e} + \dot{\gamma}_{\text{sy},e} + \dot{\gamma}_{\text{SSC},e}} \quad (31)$$

$$L_{\text{br},p} = \Omega \Gamma^2 R^2 m_p c^2 \beta c n_{\text{ISM}} \frac{\dot{\gamma}_{\text{br},p}}{\dot{\gamma}_{\text{Coul},p} + \dot{\gamma}_{\text{br},p} + \dot{\gamma}_{\text{sy},p}} \quad (32)$$

$$L_{\text{sy},e} = \Omega \Gamma^2 R^2 m_e c^2 \beta c n_{\text{ISM}} \frac{\dot{\gamma}_{\text{sy},e}}{\dot{\gamma}_{\text{M}\emptyset,e} + \dot{\gamma}_{\text{br},e} + \dot{\gamma}_{\text{sy},e} + \dot{\gamma}_{\text{SSC},e}} \quad (33)$$

$$L_{\text{sy},p} = \Omega \Gamma^2 R^2 m_p c^2 \beta c n_{\text{ISM}} \frac{\dot{\gamma}_{\text{sy},p}}{\dot{\gamma}_{\text{Coul},p} + \dot{\gamma}_{\text{br},p} + \dot{\gamma}_{\text{sy},p}} \quad (34)$$

$$L_{\text{SSC},e} = \Omega \Gamma^2 R^2 m_e c^2 \beta c n_{\text{ISM}} \frac{\dot{\gamma}_{\text{SSC},e}}{\dot{\gamma}_{\text{M}\emptyset,e} + \dot{\gamma}_{\text{br},e} + \dot{\gamma}_{\text{sy},e} + \dot{\gamma}_{\text{SSC},e}} \quad (35)$$

All luminosities have been calculated in the co-moving frame and are transformed to apparent isotropic luminosities through

$$L_{\text{app}}(\epsilon) = f_L \frac{1 - \exp^{-\tau_{\gamma\gamma}(\epsilon')}}{\tau_{\gamma\gamma}(\epsilon')} D^3 L'(\epsilon'), \quad (36)$$

where  $D = (\Gamma[1 - \beta_{\Gamma} \cos \theta_{\text{obs}}])^{-1}$  is the Doppler beaming factor,  $\epsilon = D \epsilon'$ , and  $f_L = \min(1, ct'/\Delta') \times \min(1, 1/[\Gamma^2 \Omega])$  is a correction factor accounting for the following two effects: First, due to light-travel-time constraints, only emission from a fraction of  $\sim ct'/\Delta'$  of the plasmoid will be visible to the observer. Second, if the opening angle of the cone in which plasmoid is moving, is larger than the beaming angle  $1/\Gamma$ , then only a fraction  $1/(\Gamma^2 \Omega)$  of the surface will contribute to the observed emission. In this analysis, we neglect the fact that in reality the observed emission is a superposition of emission from different layers of the plasmoid which have different evolutionary ages. This effect may alter the detailed spectral shape and light curves slightly (see, e.g., Panaitescu & Mészáros (1998) for a detailed analysis of

this effect in the case of GRB afterglows), but will not change the qualitative results of our analysis.

The effect of pair production by  $\gamma\gamma$  absorption is treated by injecting a number of thermal pairs equal to the number of absorbed photon pairs within any given time step into the plasmoid. Since we have shown that thermalization is the dominant energy-loss process for suprathermal particles, this approach yields an accurate description of the  $\gamma\gamma$  pair production process in the plasmoid.

## 5. Plasmoid deceleration

Due to momentum conservation, the bulk Lorentz factor  $\Gamma$  of the pair plasmoid will decrease as it sweeps up external matter, according to

$$d\Gamma = -\frac{(\Gamma^2 - 1) dm + \Gamma dE_{\text{adi}}}{M} \quad (37)$$

(Dermer & Humi 2001) where  $dm = \Omega R^2 (m_p + m_e) n_{\text{ISM}} \beta c dt$ ,  $dE_{\text{adi}}$  is the loss of internal energy due to adiabatic cooling, and  $M$  is the total, relativistic mass in the fireball (i. e. rest mass + internal kinetic energy of pairs + mass of swept-up external material). The rest-mass increment  $dm$  is related to the increment in  $M$  by

$$dM = \Gamma dm - \frac{dE_{\text{rad}} + dE_{\text{adi}}}{c^2} \quad (38)$$

where  $dE_{\text{rad}}$  is the net energy produced in radiation throughout the plasmoid.

## 6. Numerical results

For a general parameter study, we have performed a series of pair plasmoid simulations with various values of bulk Lorentz factors  $\Gamma$ , co-moving pair densities  $n'_{\text{pair}}$ , initial radii  $R_0$ , and external matter densities  $n_{\text{ISM}}$ . Throughout our simulations, we have fixed the magnetic field equipartition parameter to  $\epsilon_B = 0.1$ , and the observer is assumed to be located on the symmetry axis, i.e.  $\theta_{\text{obs}} = 0$ . We keep the ratio  $R/\Delta' = \Gamma_0$  constant at its initial value.

As briefly mentioned in the introduction, our simulations generally start out in a highly Thomson thick regime, in which the output is basically a thermal blackbody at the blue-shifted pair temperature. For this reason, the results are virtually independent of the initial radius  $R_0$ , and for the results presented in the following, we have chosen  $R_0 = 10^{14}$  cm.

In this initial phase, the plasmoid is inefficient in terms of high-energy emission. At the radius where the Thomson depth is  $\sim 1$ , the plasmoid becomes radiatively efficient, and a flash of high-energy  $\gamma$ -ray emission is produced. We denote the time at which the plasmoid becomes marginally Thomson-thin as  $t_T$ . This transition time is plotted as a function of the essential model parameters  $E_{\Omega,52}$  and  $\Gamma_0$  in Fig. 1 which shows that it gradually increases with increasing injected pair energy and decreasing bulk Lorentz factor. We find typical values of  $0.01 \text{ s} \lesssim t_T \lesssim 0.1 \text{ s}$ .

For each simulation, we then evaluate, among other quantities, the apparent quasi-isotropic  $\nu L_\nu$  peak luminosity and the peak photon energy  $E_{\text{pk}}$  at the time of maximum received flux. The dependence of those quantities on the parameters  $E_{\Omega,52}$  and  $\Gamma_0$  is illustrated in Figs. 2 and 3.

In these calculations, we have fixed  $n_{\text{ISM}} = 100 \text{ cm}^{-3}$ . The graphs show that we find typical peak  $\nu L_\nu$  luminosities  $\sim 10^{52} - 10^{54} \text{ ergs s}^{-1}$ , increasing with increasing  $E_{\Omega,52}$  and  $\Gamma$ .  $\nu F_\nu$  peak energies  $E_{\text{pk}}$  are typically in the range  $\sim 100 \text{ MeV} - \text{several GeV}$ , and increase with  $\Gamma$ , while they are only weakly dependent on the injected energy  $E_{\Omega,52}$ .

For a typical simulation in this range of parameters, Fig. 4 shows the composite spectrum with the individual radiation components at the time of maximum observed flux. The X-ray and  $\gamma$ -ray spectrum is clearly dominated by thermal Comptonization in this phase. time corresponding to Fig. 4, the radial Thomson depth of the plasmoid is  $\tau_T \sim 0.24$ ; the pair temperature is  $\Theta_{\text{pair}} \sim 0.44$ . The spiky shape of the electron and proton synchrotron spectra is due to the  $\delta$  function approximation to the respective emissivities.

Fig. 5 illustrates the spectral evolution during the collision dominated phase of the pair plasmoid evolution. It shows that the hard X-ray and  $\gamma$ -ray spectral output remains dominated by thermal Comptonization throughout most of this phase. During the first few ms, there is a strong soft X-ray component due to the thermal emission of the cold pair plasmoid, which is rapidly shifting to higher energies as the pairs are being heated. At very high energies,  $E \gtrsim 1 \text{ GeV}$ , there is a weak tail from suprathermal proton bremsstrahlung. According to Eq. (1), hydromagnetic turbulence might develop within  $\sim 1 \text{ s}$  in the case discussed here.

Light curves expected from the collision-dominated pair plasmoid are shown in Fig. 7. The figure illustrates that the maximum spectral power output is expected around  $\sim 0.1 \text{ s}$  after the formation of the pair plasmoid. Generally, the time of maximum flux decreases with increasing photon energy, indicating an overall hard-to-soft spectral evolution.

## 7. Summary and conclusions

We have investigated the early stages of the evolution of a relativistic pair fireball, immediately after it has become optically thin to  $\gamma\gamma$  pair production. We have shown that for a short period of time,  $\sim 0.1$  – a few seconds after the initial explosion, the pair blast wave evolution might be dominated by collisional processes prior to the formation of a collisionless shock which would subsequently lead to non-thermal particle acceleration at the shock front. We have simulated the relevant energy exchange and radiation processes, including suprathermal electron and proton thermalization and bremsstrahlung, suprathermal electron and proton synchrotron emission, thermal pair bremsstrahlung, thermal pair annihilation, thermal Comptonization, and  $\gamma\gamma$  pair production and absorption, during the early pair plasmoid evolution, and calculated the expected radiative signatures.

We have investigated the dependence of the radiative signatures on pair plasmoid parameters which are very hard to predict from first principles in the framework of current GRB progenitor models. In the range of total injected energies of  $E_\Omega \sim 10^{52}$  ergs sr $^{-1}$  and initial bulk Lorentz factors  $\Gamma_0 \sim 500 - 1000$ , the radiation from the collision-dominated pair plasmoid phase results in a short period ( $\sim$  a few ms) of thermal soft X-ray emission from the initially Thomson thick, cold pair plasmoid. As the pair plasma is heated due to the sweeping-up of external material and is becoming Thomson thin due to expansion, the observable emission turns into a quasi-thermal spectrum, peaking at around  $E_{\text{pk}} \sim 100$  MeV – a few GeV, dominated by thermal Comptonization by the mildly relativistic pair plasma in the plasmoid during the first  $\sim 0.01 - 1$  sec after the onset of the GRB. The apparent peak  $\nu L_\nu$  luminosities are expected in the range of  $\sim 10^{52} - 10^{54}$  ergs/s, sustained over typically a few tens of milliseconds.

The expected very early, thermal signatures may already have been observed in time-resolved, early BATSE spectra of a few GRBs. The quasi-thermal spectra expected during the optical-thinning transition phase,  $\sim 0.01 - 1$  s after the onset of the GRB, are peaking in the  $\sim 100$  MeV regime. Thus, they may have remained undetectable for BATSE, but should be easily detectable by the GLAST mission, scheduled for launch in 2005.

We thank the anonymous referee for helpful and constructive comments, and Dr. C. D. Dermer for careful reading of the manuscript and stimulating discussions. The work of MB is supported by NASA through Chandra Postdoctoral Fellowship grant PF 9-10007 awarded by the Chandra X-ray Center, which is operated by the Smithsonian Astrophysical Observatory for NASA under contract NAS 8-39073. RS acknowledges partial support by the Bundesministerium für Bildung und Forschung through DESY, grant 05AG9PCA.

### A. Bremsstrahlung losses of suprathermal protons

In order to calculate the energy loss rate of suprathermal electrons due to bremsstrahlung in inelastic collisions with a cold pair plasma, we start out with the differential cross section  $\frac{d\sigma}{d\epsilon}$  as given in Eq. (4) of Jones (1971) (for consistency we use  $\epsilon$  for the normalized energy of the outgoing photon, which is  $\alpha$  in Jones' notation) and evaluate

$$\dot{\gamma}_{\text{br,p}} = -n'_e \beta_p c \frac{m_e}{m_p} \int_0^{\epsilon_{\text{max}}} d\epsilon \epsilon \frac{d\sigma}{d\epsilon} \quad (\text{A1})$$

where

$$\epsilon_{\text{max}} = 1.123 \gamma_p \beta_p^2 e^{-\frac{\beta_p^2}{2}}. \quad (\text{A2})$$

Evaluating the integral in (A1), we find

$$\dot{\gamma}_{\text{br,p}} = -\frac{3 \sigma_T \alpha c m_e}{4 \pi} \frac{n'_e}{m_p \beta_p} G(\gamma_p) \quad (\text{A3})$$

where  $\alpha \approx 1/137$  is the fine structure constant, and

$$G(\gamma_p) = \frac{2}{3} (\ln A)^2 + \left( \frac{4}{3} \ln 2 + \frac{13}{18} \right) \ln A + \frac{190}{27} - \frac{2}{9} \pi^2 + \frac{19}{40} \ln 2 + O\left(\frac{1}{A}\right), \quad (\text{A4})$$

where  $A \approx 0.68 \gamma_p \gg 1$  for relativistic protons. The last term in Eq. (A4) denotes all terms of order  $1/A \ll 1$ .

### B. The electron-SSC spectrum

We evaluate the electron-SSC spectrum using a  $\delta$  function approximation for the Compton scattering cross section in the Thomson regime (Reynolds 1982), with a sharp cut-off at incident photon energies  $\epsilon \gamma_e \geq 1$ . In the case  $\gamma_e^{\text{br}} = \Gamma$  this yields:

$$L_{\text{SSC}}(\epsilon) = L_{\text{SSC}}^0 \epsilon^{1/3} \left( \Gamma^{1/3} - \Gamma^{-1/3} \left[ \frac{3}{4} \epsilon \frac{B_{\text{cr}}}{B} \right]^{1/6} \right) \Theta \left( \frac{4}{3} \Gamma^4 \frac{B}{B_{\text{cr}}} - \epsilon \right) \quad (\text{B1})$$

In the case  $\gamma_e^{\text{br}} < \Gamma$ , we find:

$$L_{\text{SSC}}(\epsilon) = L_{\text{SSC}}^0 \cdot \begin{cases} 3 \left(\frac{4}{3}\right)^{2/3} \left(\frac{\epsilon}{\epsilon_{\text{sy,e}}^{\text{br}}}\right)^{1/3} (\gamma_e^{\text{br}})^{1/3} \\ \cdot \left(1 + \frac{1}{5} \left[1 - \left\{\frac{\gamma_e^{\text{br}}}{\Gamma}\right\}^{5/3}\right]\right) \\ - \frac{5}{2} \left(\frac{4}{3}\right)^{1/2} \left(\frac{\epsilon}{\epsilon_{\text{sy,e}}^{\text{br}}}\right)^{1/2} \left(1 + \frac{1}{5} \left[\frac{\gamma_e^{\text{br}}}{\Gamma}\right]^2\right) & \text{if } \frac{4}{3}\epsilon_{\text{sy,e}}^{\text{max}} \leq \epsilon \leq \frac{4}{3}(\gamma_e^{\text{br}})^2 \epsilon_{\text{sy,e}}^{\text{br}} \\ \frac{11}{10} \left(\frac{4}{3}\right)^{3/2} \left(\frac{\epsilon}{\epsilon_{\text{sy,e}}^{\text{br}}}\right)^{-1/2} (\gamma_e^{\text{br}})^2 \\ - \frac{1}{2} \left(\frac{4}{3}\right)^{1/2} \left(\frac{\epsilon}{\epsilon_{\text{sy,e}}^{\text{br}}}\right)^{1/2} \left(\frac{\gamma_e^{\text{br}}}{\Gamma}\right)^2 \\ - \frac{3}{5} \left(\frac{4}{3}\right)^{2/3} \left(\frac{\epsilon}{\epsilon_{\text{sy,e}}^{\text{br}}}\right)^{1/3} \frac{(\gamma_e^{\text{br}})^2}{\Gamma^{5/3}} \\ + \frac{1}{2} \left(\frac{4}{3}\right)^{3/2} \left(\frac{\epsilon}{\epsilon_{\text{sy,e}}^{\text{br}}}\right)^{-1/2} (\gamma_e^{\text{br}})^2 \ln\left(\frac{3\epsilon}{4\epsilon_{\text{sy,e}}^{\text{br}}[\gamma_e^{\text{br}}]^2}\right) & \text{if } \frac{4}{3}(\gamma_e^{\text{br}})^2 \epsilon_{\text{sy,e}}^{\text{br}} \leq \epsilon \leq \frac{4}{3}(\gamma_e^{\text{br}})^2 \epsilon_{\text{sy,e}}^{\text{max}} \\ \frac{1}{2} \left(\frac{4}{3}\right)^{3/2} \left(\frac{\epsilon}{\epsilon_{\text{sy,e}}^{\text{br}}}\right)^{-1/2} (\gamma_e^{\text{br}})^2 \ln\left(\frac{4\epsilon_{\text{sy,e}}^{\text{max}} \Gamma^2}{3\epsilon}\right) & \text{if } \frac{4}{3}(\gamma_e^{\text{br}})^2 \epsilon_{\text{sy,e}}^{\text{max}} \leq \epsilon \leq \frac{4}{3}\Gamma^2 \epsilon_{\text{sy,e}}^{\text{max}} \end{cases} \quad (\text{B2})$$

The integrated luminosity in this spectrum is

$$L_{\text{SSC,e}} = L_{\text{SSC}}^0 N \quad (\text{B3})$$

where

$$N = \begin{cases} \frac{1}{9} \left(\frac{4}{3}\right)^{1/3} \Gamma^{17/3} \left(\frac{B}{B_{\text{cr}}}\right)^{4/3} & \text{if } \gamma_e^{\text{br}} = \Gamma \\ \left\{ \left(\frac{4}{3}\right)^2 \epsilon_{\text{sy,e}}^{\text{br}} (\gamma_e^{\text{br}})^3 \right\} \left\{ \frac{5}{6} - \frac{27}{10} \left(\frac{\Gamma}{\gamma_e^{\text{br}}}\right)^{8/3} + \frac{9}{20} \left(\frac{\Gamma^3}{[\gamma_e^{\text{br}}]^{11}}\right)^{1/3} \right. \\ \left. + \frac{5}{3} \left(\frac{\Gamma}{[\gamma_e^{\text{br}}]^2}\right)^3 + \frac{1}{3} \frac{\Gamma}{(\gamma_e^{\text{br}})^4} - \frac{31}{12} \frac{\Gamma}{\gamma_e^{\text{br}}} + 2 \left(\frac{\Gamma}{\gamma_e^{\text{br}}}\right)^2 \right\} & \text{if } \gamma_e^{\text{br}} < \Gamma \end{cases} \quad (\text{B4})$$

## REFERENCES

- Band, D. L., et al., 1993, ApJ, 413, 281  
 Böttcher, M., & Dermer, C. D., 2000, ApJ, 532, 281  
 Böttcher, M., Pohl, M., & Schlickeiser, R., 1999, Astrop. Phys., 10, 47  
 Brainerd, J. J., 1994, ApJ, 428, 21



- Cavallo, G., & Rees, M. J., 1978, MNRAS, 183, 359
- Crider, A. W., et al., 1997, ApJ, 479, L39
- Galama, T. J., Wijers, R. A. M. J., Bremer, M., Groot, P. J., Strom, R. G., Kouveliotou, C., & van Paradijs, J., 1998, ApJ, 500, L97
- Dermer, C. D., Böttcher, M., & Chiang, J., 2000, ApJ, 537, 255
- Dermer, C. D., & Humi, M., 2001, ApJ, submitted
- Dermer, C. D., & Mitman, K. E., 1999, ApJ, 513, L5
- Fenimore, E. E., Madras, C. D., & Nayakshin, S., 1996, ApJ, 473, 998
- Hua, X.-M., & Titarchuk, L., 1995, ApJ, 449, 188
- Jones, F., C., 1971, ApJ, 169, 503
- Katz, J. I., 1994, ApJ, 432, L107
- Liang, E. P., 1997, ApJ, 491, L15
- Mannheim, K., & Schlickeiser, R., 1994, A&A, 286, 983
- Mészáros, P., Laguna, P., & Rees, M. J., 1993, ApJ, 416, 181
- Mészáros, P., & Rees, M. J., 1993, MNRAS, 257, 29P
- Mészáros, P., & Rees, M. J., 1993, ApJ, 418, L59
- Mészáros, P., Rees, M. J., & Wijers, R. A. M. J., 1998, ApJ, 499, L301
- Nayakshin, S., & Melia, F., 1998, ApJS, 114, 269
- Paczyński, B., & Rhoads, J., 1993, ApJ, 418, L5
- Panaitescu, A., & Mészáros, P., 1998, ApJ, 493, L31
- Pohl, M., & Schlickeiser, R., 2000, A&A, 354, 395
- Preece, R. D., et al., 1997, ApJ, 506, L23
- Preece, R. D., 2001, in proc. of Ninth Marcell Grossmann Meeting, in press
- Rees, M. J., & Mészáros, P., 1992, MNRAS, 258, 41P

- Reynolds, S. P., 1982, *ApJ*, 256, 38
- Sari, R., & Esin, A. A., 2001, *ApJ*, 548, 787
- Sari, R., & Piran, R., 1997, *ApJ*, 485, 270
- Sari, R., Piran, T., & Narayan, R., 1998, *ApJ*, 497, L17
- Schlickeiser, R., & Dermer, C. D., 2000, *A&A*, 360, 789
- Schlickeiser, R., Schuster, C., Böttcher, M., Lerche, I., & Pohl, M., 2001, in preparation
- Shemi, A., & Piran, T., 1990, *ApJ*, 365, L55
- Svensson, R., 1982, *ApJ*, 258, 321
- Tavani, M., 1996, *Phys. Rev. Lett.*, 78 (23), 4328
- Vietri, M., 1997, *ApJ*, 478, L9
- Waxman, E., 1997, *ApJ*, 485, L5
- Wijers, R. A. M. J., Rees, M. J., & Mészáros, P., 1997, *MNRAS*, 288, L51

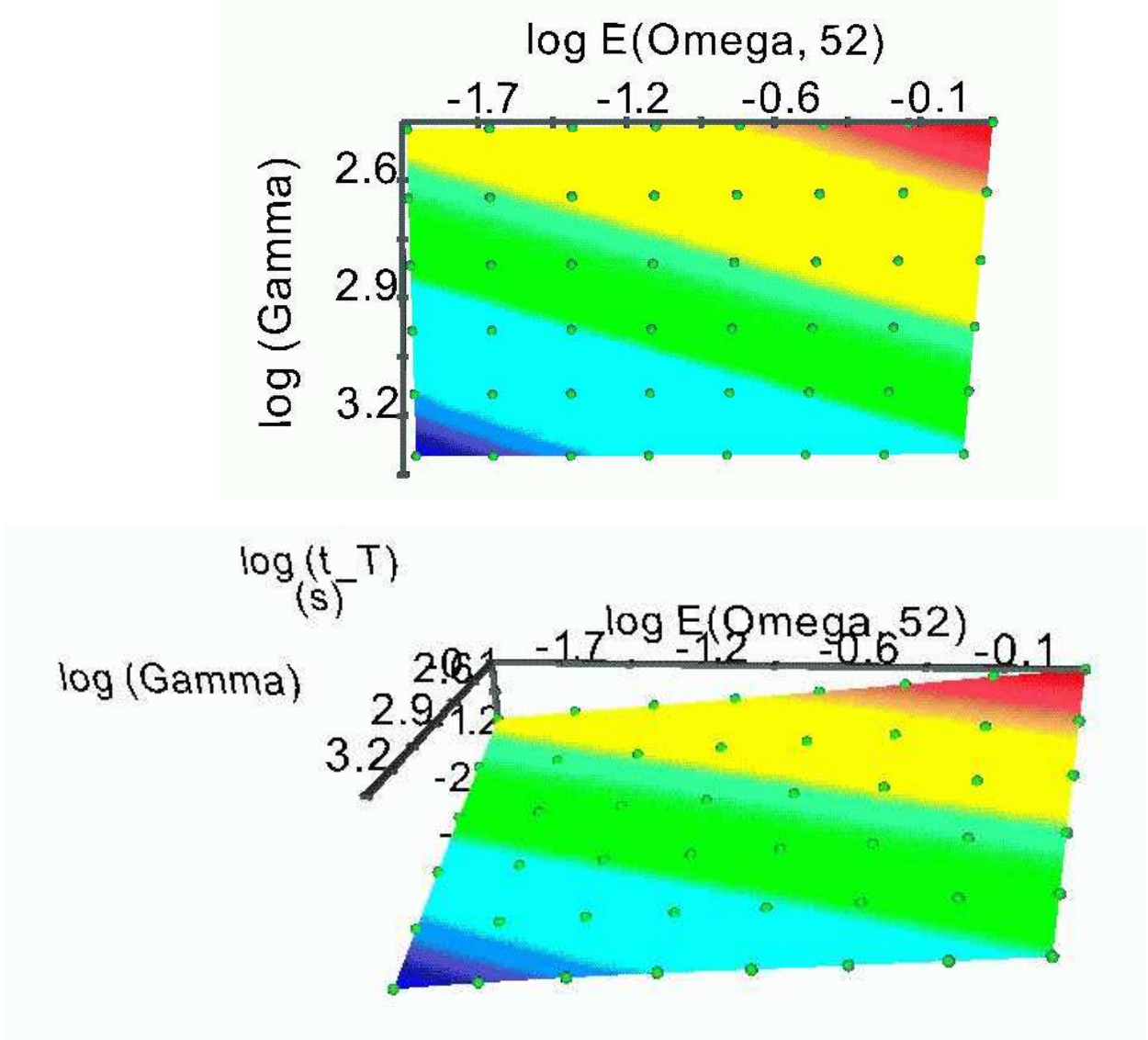


Fig. 1.— Thomson thinning time  $t_T$  of a relativistic pair plasmoid injected at  $R_0 = 10^{14}$  cm, as a function of total injected energy per unit solid angle,  $E_\Omega$ , and initial bulk Lorentz factor  $\Gamma_0$ . Other parameters:  $n_{\text{ISM}} = 100$ , and  $R/\Delta' = \Gamma$ . The green dots indicate simulated values; the surface has been constructed using a spline interpolation. The surface colors encode the values of  $t_T$  (vertical axis in the lower panel) with red corresponding to  $t_T \sim 0.5 - 1$  s and blue corresponding to  $t_T \sim 0.5 - 1$  ms.

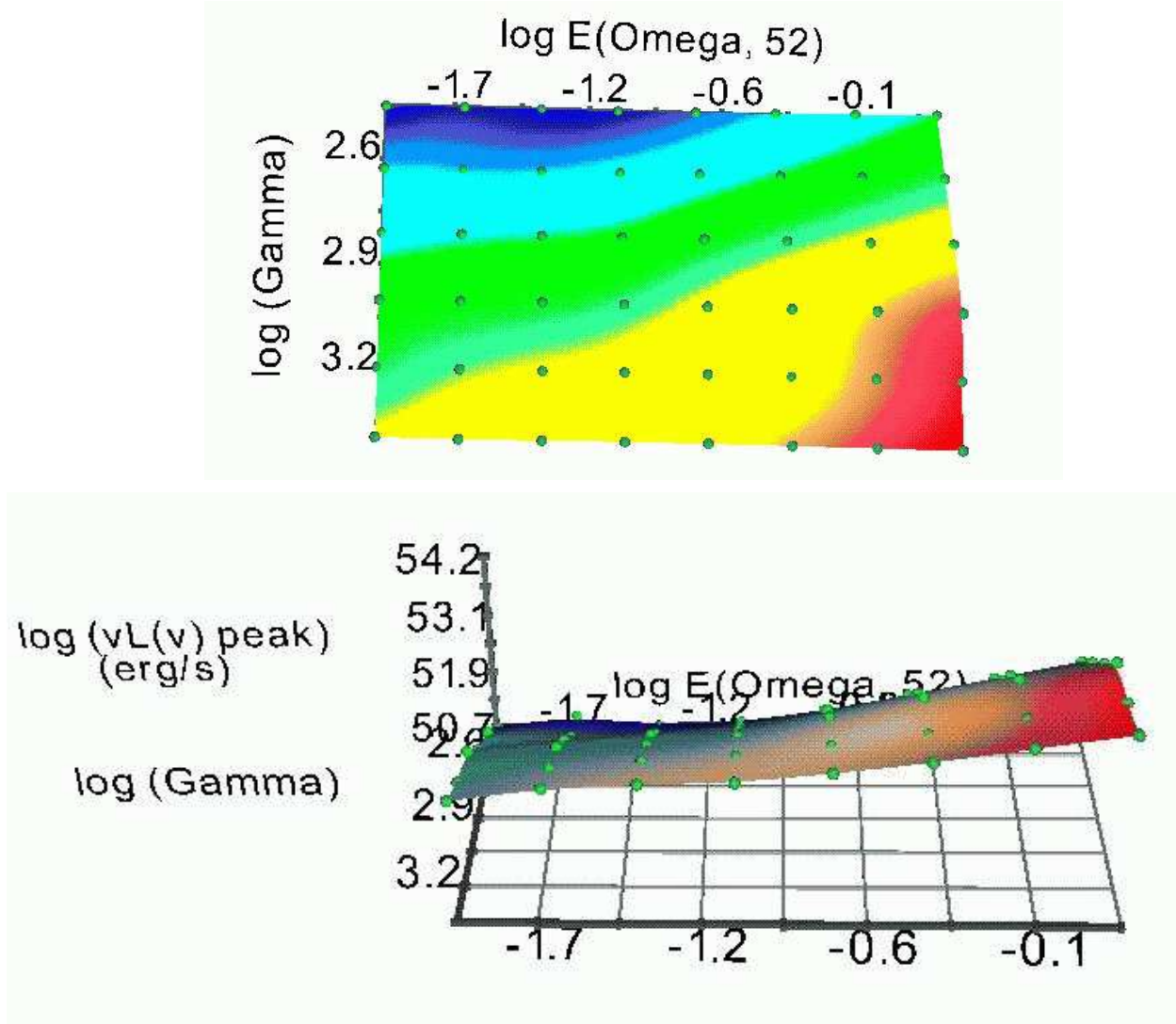


Fig. 2.— Peak  $\nu L_{\nu}$  apparent isotropic luminosity at the time of maximum received flux, as a function of  $E_{\Omega,52}$  and  $\Gamma_0$ . Parameters are the same as in Fig. 1. The green dots indicate simulated values. The surface colors encode the values of  $\nu L_{\nu, \text{peak}}$  with red corresponding to  $\nu L_{\nu, \text{peak}} \sim 10^{54}$  ergs s $^{-1}$  and blue corresponding to  $\nu L_{\nu, \text{peak}} \sim 10^{51}$  ergs s $^{-1}$ .

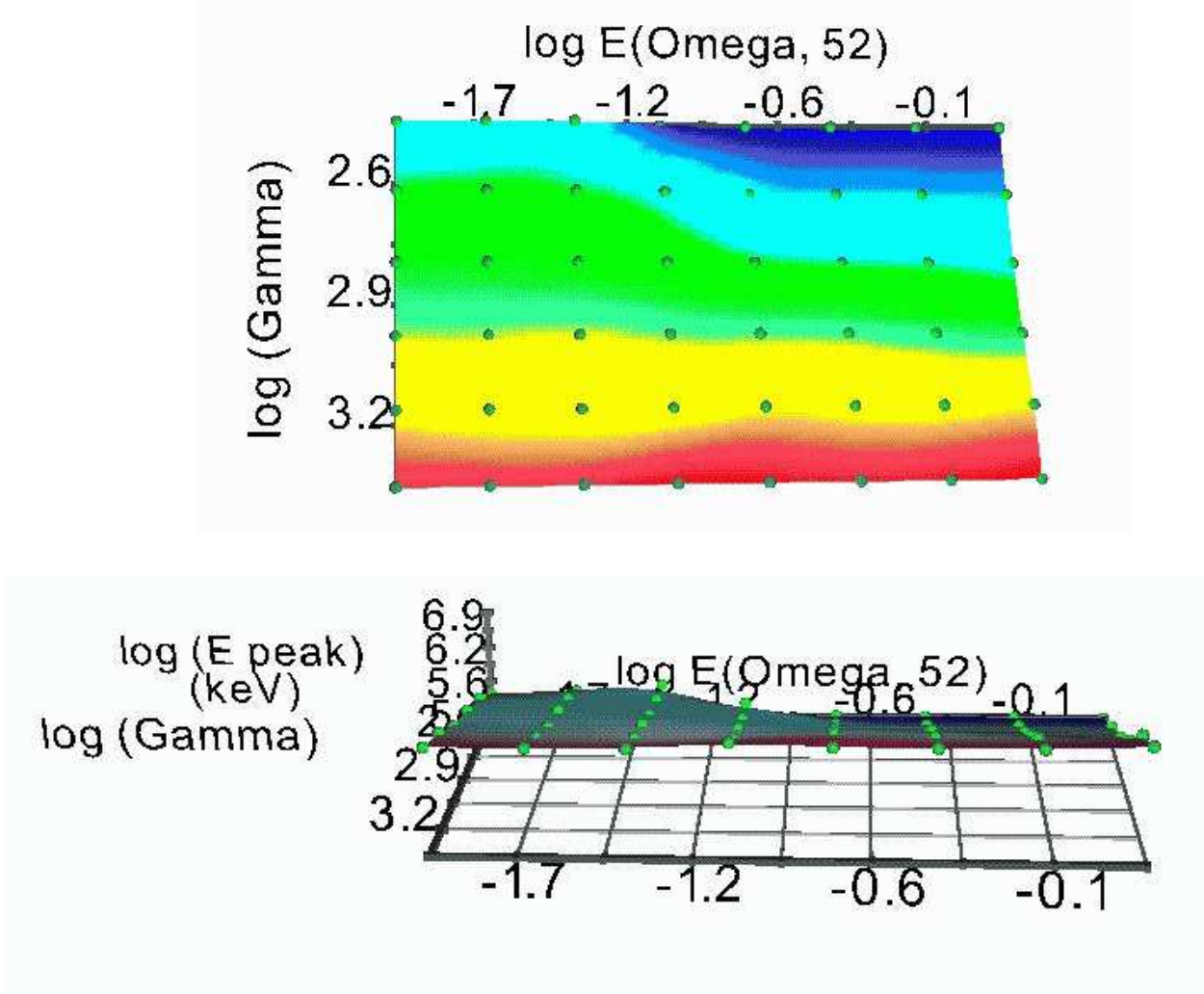


Fig. 3.— Peak photon energy at the time of maximum received flux, as a function of  $E_{\Omega,52}$  and  $\Gamma_0$ . Parameters are the same as in Fig. 1. The green dots indicate simulated values. The surface colors encode the values of  $E_{\text{peak}}$  with red corresponding to  $E_{\text{peak}} \sim 10$  GeV and blue corresponding to  $E_{\text{peak}} \sim 100$  MeV.

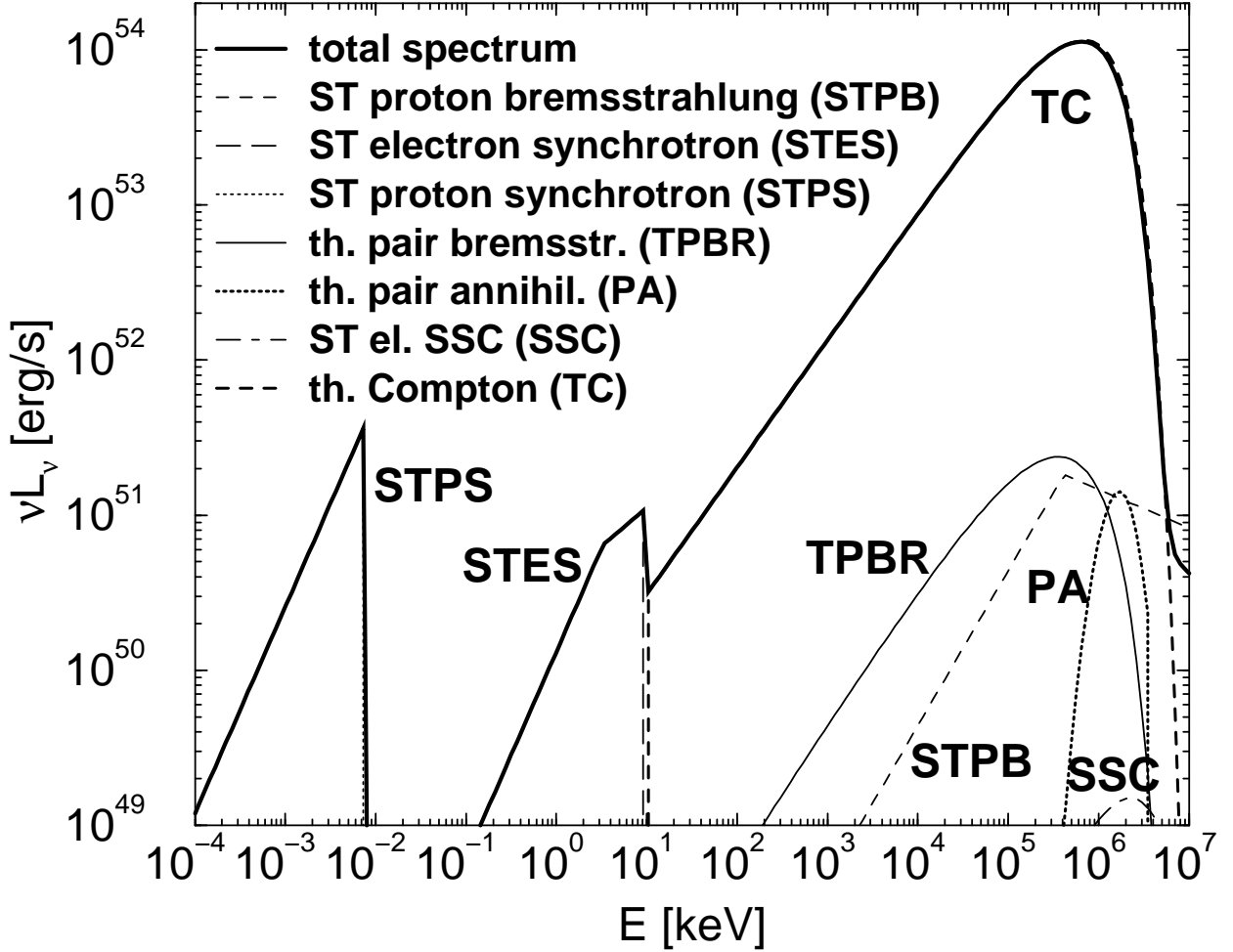


Fig. 4.— Composite photon spectrum from the blast wave at the time of maximum received flux ( $t_{\text{rec}} = 64$  ms). Parameters for this simulation are:  $\Gamma_0 = 10^3$ ,  $n'_{\text{pair}} = 1.2 \times 10^{16} \text{ cm}^{-3}$ ,  $R_0 = 10^{14} \text{ cm}$ , implying  $E_{\Omega,52} = 1$ ;  $n_{\text{ISM}} = 100 \text{ cm}^{-3}$ ,  $\epsilon_B = 0.1$ ,  $\theta_{\text{obs}} = 0$ .  $\gamma\gamma$  absorption has been taken into account to calculate the total emission, while the individual contributions are plotted without correction for  $\gamma\gamma$  absorption. Thus, the importance of  $\gamma\gamma$  absorption and pair production is illustrated by the difference between the individual, unabsorbed components and the total, emerging spectrum at  $E \gtrsim 1 \text{ GeV}$ .

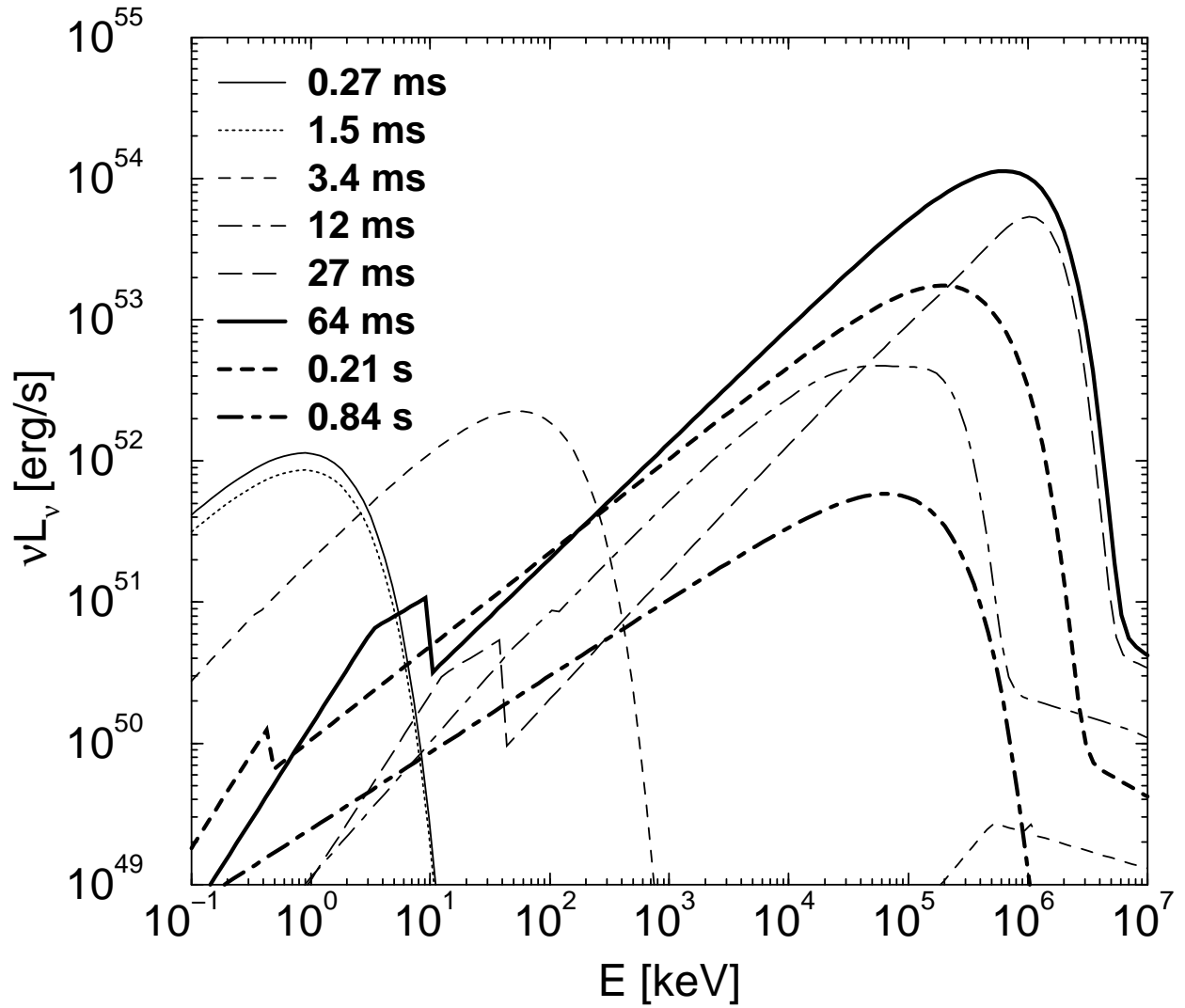


Fig. 5.— Time evolution of the observed photon spectra for the same set of parameters as in Fig. 4.

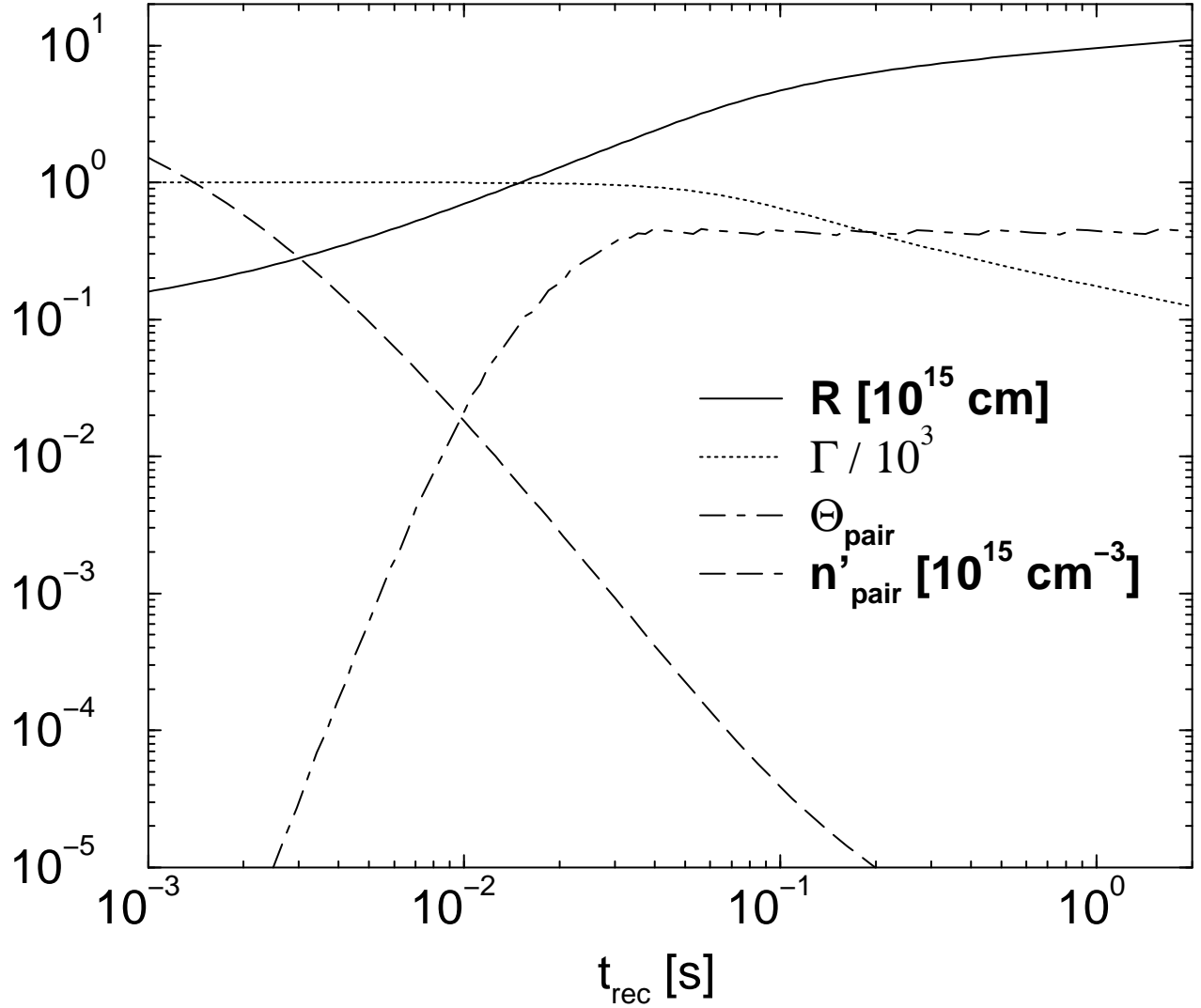


Fig. 6.— Time evolution of several relevant quantities describing the evolution of the plas-  
moid, for the same set of parameters as in Fig. 4.



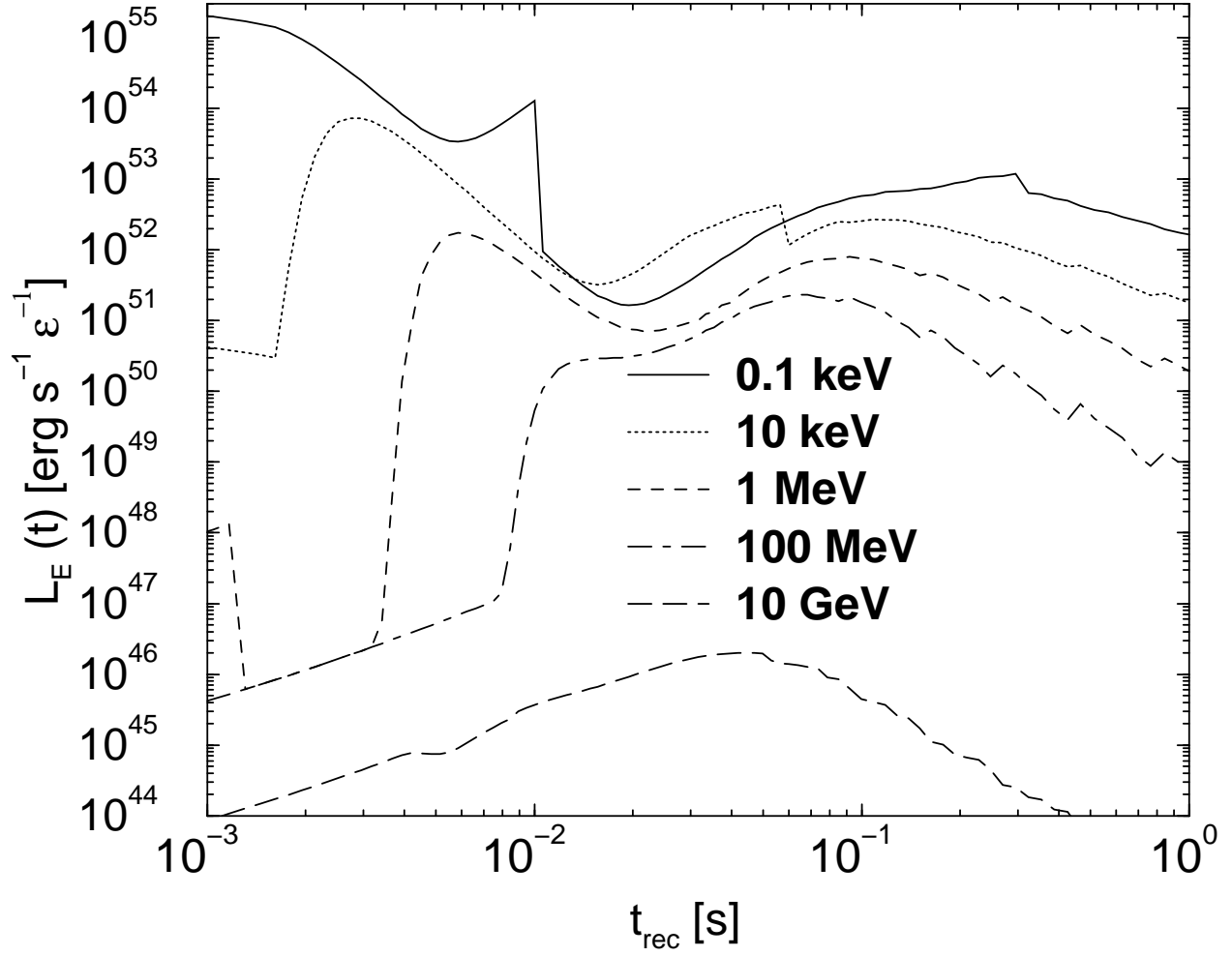


Fig. 7.— Light curves at several different observed photon energies for the same set of parameters as in Fig. 4.